DIRECT CALCULATION OF DYNAMIC RELATIVE PERMEABILITIES FROM *IN-SITU* PHASE PRESSURES AND FLUID SATURATIONS

Brattekås, B., Brautaset, A., Haugen, Å., Graue, A.
Department of Physics and Technology, University of Bergen, Norway

This paper was prepared for presentation at the International Symposium of the Society of Core Analysts held in Napa Valley, California, USA, 16 – 19 September, 2013.

ABSTRACT

This work experimentally investigated an improved method for extracting two-phase relative permeability from dynamically measured *in-situ* capillary pressures and fluid saturations. High resolution Magnetic Resonance Imaging (MRI) for three-dimensional saturation monitoring, and local phase pressure measurements from two oil-wet and two water-wet semi-permeable discs implemented along the core length were used to monitor flow functions during unsteady state waterfloods in low permeable chalk. Combining measured phase pressures with Darcy velocities calculated from *in-situ* saturation gives a direct measure of relative permeability and reduces the time delay significantly compared to conventional unsteady state experiments. Imbibition relative permeabilities were calculated individually over a large saturation range for the oil and water phases in strongly water-wet and neutral-wet core samples, without using capillary pressure approximations.

INTRODUCTION

Accurate description of two-phase flow functions in porous media is important in order to estimate recovery and flow interactions in a reservoir, and experimentally verified input relative permeability curves for core flood and reservoir simulators are in demand. Traditionally, core flood experiments to extract relative permeabilities do not reflect true reservoir conditions: steady state experiments mix drainage and imbibition processes, and unsteady state methods traditionally make use of the core differential pressure and production data to describe pressure gradients and average core saturation, and estimates two-phase flow functions using the JBN method [1] or similar [2]. The approximations implied in the calculations are coarse, and especially the high flow rates that must be used in order to neglect capillary pressure, end effects and pressure changes across the displacement front, disagree with realistic reservoir flow rates. Incorporation of capillary effects is essential to extract trustworthy relative permeability curves from low flow rate experiments.

To improve the measurement and extraction of two-phase flow functions, utilization of local *in-situ* measurements of saturation and/or fluid phase pressures have been discussed [3]-[12]. Most methods measure either saturation or pressure *in-situ*, and use numerical methods to estimate the other, and ultimately relative permeability. Few authors have yet presented experimental results utilizing *in-situ* measurements of both pressure and saturation [3], [7] and even fewer have investigated simultaneous *in-situ* measurements of individual phase pressures and saturation [9], [13], which may be used to explicitly calculate relative permeabilities for each immiscible fluid phase.

EXPERIMENTAL PROCEDURES

Three Portland chalk core samples [14] were dried at 80 °C, vacuum evacuated and saturated with synthetic brine. Porosity was determined from weight measurements and permeability to brine was calculated using Darcy's law. Two cores were aged [15] in crude oil at 80 °C for 6 days to obtain neutral-wet conditions, measured using the Amott method [16]. Fluids used are listed in Table 1, and core properties are listed in Table 2.

The cores were prepared for MRI imaging by substituting Ekofisk brine with deuterium oxide (D_2O) brine, so that oil saturation could be determined from the measured MRI intensities. N-Decane was injected at constant pressure (200 kPa/cm) to the irreducible water saturation, S_{wi}. The cores were epoxy-coated at S_{wi} with Polyoxymethylene (POM) end pieces mounted on the inlet and outlet ends. Four 1.2 cm diameter holes were drilled through the epoxy at two selected positions along the core length, two on each side of the core, and 1.1 cm diameter semi-permeable discs with oil-wet or water-wet wetting preference were placed in the holes. Nylon elbow connectors were glued to the discs, and the space between the elbow connectors and the epoxy was filled with silicone and topped with a new layer of epoxy to prevent leaks.

The cores were mounted in the MRI and waterflooded from S_{wi} at constant injection pressures of 69 kPa (Core 1) and 34.5 kPa (Core 2), or constant injection rate of 2 ml/h (Core 3). *In-situ* phase pressures and fluid saturations were monitored as functions of time and position using MRI imaging and computer logged Validyne pressure transducers. The pressure ports were aligned horizontally to minimize gravity effects. MRI images were collected at desired time steps during the waterfloods, and fluid saturations were extracted from the MRI intensities by normalizing average longitudinal 2D intensities to the effluent production data. The local oil saturations at the pressure ports were calculated from the transverse cross section of the core at P_1 (Port 1, oil-wet and water-wet phase pressure ports closest to the inlet) and P_2 (Port 2, second set of oil- and water-wet pressure ports) locations, thus reducing the time delay experienced in conventional measurement methods, in which saturation is calculated as an average of small length segments of the cores. The experiments were terminated when the pressure in all ports was constant with time. Figure 1 shows the experimental setup for core flooding in the MRI.

EXPERIMENTAL RESULTS AND APPLICATIONS

Figure 2 shows oil saturations and local fluid phase pressures for strongly water-wet Core 1 at P_1 and P_2 locations during waterflooding. The oil phase immediately responded to the applied injection pressure and phase pressures in both oil-wet ports increased to reach a maximum of 41.4 kPa in P_1 and 16.5 kPa in P_2, before decreasing to 24.1 kPa in P_1 and 4.1 kPa in P_2 as the water front passed the port locations. During imbibition, oil saturations decreased from 68 to 30 %PV at P_1 and from 69 to 35 %PV at P_2 locations, while water phase pressures slowly increased from 0 to 37.9 kPa and 4.4 kPa in P_1 and P_2, respectively. The moveable oil volume was approximately 33% of the total core pore volume (PV); the sudden increase in phase pressures at t=0.35 PV injected may thus be a sign of the water front reaching the outlet end and accumulating there before breakthrough, increasing the local water saturation and the

resistance for oil to be produced, due to sudden low oil relative permeability. The manifestation of this capillary end effect was seen as pressure build-up in both fluid phases. The build-up occurred after the saturation shock passed P_1 and P_2 locations and was thus not included in relative permeability calculations. Dynamic capillary pressure was given directly at each port location from the phase pressure measurements. Zero capillary pressure was reached at t=0.24 PV (Sw≈0.6) and marks the change in production regime from spontaneous to forced imbibition.

Figure 3 shows local oil saturations and separate phase pressures during waterflooding of Core 2. The oil phase immediately responded to the applied differential pressure and increased to reach maximum oil pressure of 21.8 kPa in P_1 and 7.9 kPa in P_2. From t = 0.04 - 0.35 PV injected, the oil pressure declined from 20.0 kPa to 0 in P_1. In P_2, pressure decreased to 2.7 kPa at t=0.15 PV and thereafter increased to 31.0 kPa. From t=0.04-0.39 PV water pressures increased from 3.4 kPa to 31.0 kPa in P_1 and 0 to 27.6 kPa in P_2. Core 2 was of near neutral wettability and did therefore not imbibe significant amounts of water, or retain water at the outlet end of the core before production. Spontaneous imbibition of water ended at t = 0.11 PV (Sw≈0.4). The oil saturations decreased from 72 to 44 %PV in P_1 and from 71 to 40 %PV in P_2. The development in P_2 oil phase pressure was comparable to P_2 water phase pressure, and indicates that the oil-wet pressure disk may be faulty. The measured P_1 capillary pressure and P_2 water pressure was therefore used to calculate P_2 oil pressure and subsequently relative permeability.

Figure 4 shows oil saturations and local separate phase pressures for Core 3 at P_1 and P_2 locations during waterflooding. The oil pressures increased from 0 to 30.5 kPa in P_1 and from 0.5 to 25.6 kPa in P_2 as the water front passed the ports, and the water pressures increased from -2.8 kPa to 71.1 kPa in P1 and from 0.5 kPa to 60.9 kPa in P_2. The oil saturation decreased from 76 to 33 %PV in P_1 and from 73 to 33 %PV in P_2. The core was at neutral-wet conditions, and recovery from spontaneous imbibition ended at t=0.1 PV (Sw≈0.7), where zero capillary pressure was reached. Negative pressures were observed in water-wet P_1 and oil-wet P_2 before and after the displacement front passed, respectively. As the negative values occur outside of the saturation shock, they are not included in the calculations of relative permeability.

Relative permeabilities were explicitly calculated from (1) and (2) using the measured *in-situ* pressure and saturation data, and the calculation method developed by Kolltveit *et al.* [3]. The phase pressures were separately measured in our experiments, which is a new addition to this method. Obtaining Darcy velocities for each fluid phase as continuous functions of saturation was not straight forward and a few assumptions were made: 1) before the saturation front passes the port location ($S_w = S_{wi}$), $u_w = 0$, and 2) after the front passes ($S_w = 1\text{-}S_{or}$), $u_w = u_{tot}$. 3) In the transient period, $u_w(S_w)$, and may be determined from *in-situ* saturation measurements in P_1 and P_2 using the equation of continuity (3), and (4). The corresponding u_o may then be calculated (5):

$$k_{rw}(S) = -\frac{\mu_w}{K} \cdot \frac{u_w}{\frac{P_w^S(P_2,t_2) - P_w^S(P_1,t_1)}{\Delta x}} \quad (1)$$

$$k_{ro}(S) = -\frac{\mu_o}{K} \cdot \frac{\frac{q_w}{A} - u_w}{\frac{P_o^S(P_2,t_2) - P_o^S(P_1,t_1)}{\Delta x}} \quad (2)$$

$$\int_{x_1}^{x_2} \frac{\partial u_w}{\partial x} dx = -\int_{x_i}^{x_2} \frac{\partial S_w}{\partial t} dx = \varphi \cdot \int_{x_1}^{x_2} v(S_w) \cdot \frac{\partial S_w}{\partial x} dx \quad (3)$$

$$u_w(x_2,t) = u_w(x_1,t) - v_{ave} \cdot \varphi \cdot \{S_w(x_1,t) - S_w(x_2,t)\} \quad (4)$$

$$u_o(x_2,t) = u_{tot} - u_w(x_2,t) = \frac{q_w}{A} - u_w(x_2,t) \quad (5)$$

The main approximation is to introduce an average water front velocity, v_{ave}, which was directly extracted from *in-situ* saturation data at P_1 and P_2 and, together with porosity, defines the slope of a linear relationship between u_w and S_w. Non-linear deviations from the linear solution were investigated by imposing a 10% discrepancy at intervenient water saturations and decreasing towards saturation endpoints (S_{wi} and S_{or}). The calculated relative permeabilities are plotted in Figure 5 for Core 1, Figure 6 for Core 2 and Figure 7 for Core 3. The black lines in the figures represent relative permeabilities from linearly calculated u_w, and the dotted lines represent under- and over estimates. Non-linear Darcy velocities impacted the relative permeabilities to a minor extent, and deviations were measured to maximum 0.03 for Core 1 and <0.007 for Core 2 and Core 3. The higher deviation in the strongly water-wet case follows from significantly higher u_w, due to capillary driven suction of water.

A comparison with conventional steady-state relative permeabilities for a strongly water-wet chalk core is shown for Core 1 [17] in Figure 6 and reveals similarly shaped relative permeability curves, although only oil relative permeability values agree. The water relative permeability values are quite high in this study, caused by spontaneous imbibition of water into the core, which increased u_w and thus k_{rw}. In a steady state experiment, the spontaneous imbibition is suppressed because the fluid flow is a mix between drainage and imbibition processes. Some differences in curve behavior may also be expected due to the dynamically measured capillary pressure applied in this method compared to the static pressure data used in conventional relative permeability calculations. The applied differential pressures and flow rates in this study are quite low compared to conventional unsteady state experiments on this core material, and yielded low relative permeabilities below 16% of the effective phase permeabilities in the neutral wet cases. The extracted relative permeability curves were consistent with wettability and in accordance with the rules of thumb by Craig [18].

The main experimental challenge is achieving reliable phase pressure measurements simultaneously with *in-situ* saturation. When using the MRI setup, Validyne pressure transducers were positioned outside the immediate MRI area, hence large tubing volumes were required to connect pressure ports and transducers. The pressure ports provide reliable pressures measurements in most cases, but negative pressures were also observed.CONCLUSIONS

Local phase pressures and *in-situ* saturation measurements in three Portland chalk cores at different wettabilities have been obtained during waterfloods using high spatial resolution MRI and *in-situ* measurements of phase pressure. Using the

measured data for relative permeability calculations ensured minimal influence from end effects and limited the need for transient production data, allowing a larger saturation range than conventional unsteady state methods.

ACKNOWLEDGEMENTS

The authors wish to thank Jim Stevens at the ConocoPhillips Research Center in Bartlesville, OK, USA, for his contributions during the experiments. Three of the authors are indebted to the Norwegian Research Council for financial support.

NOMENCLATURE

A	=	*Cross-sectional area*	R_f	=	*Recovery factor*
φ	=	*Porosity*	S	=	*Saturation*
I_w	=	*Amott Index to water*	t	=	*Time*
K	=	*Absolute permeability*	Δt^S	=	*Time for one saturation to travel Δx*
k_r	=	*Relative permeability*	u	=	*Darcy velocity*
μ	=	*Viscosity*	u_{tot}	=	*Total Darcy velocity*
o	=	*(Subscript) Oil*	v_{ave}	=	*Average front velocity*
w	=	*(Subscript) Water*	$v(S_w)$	=	*Velocity at given Sw between two selected points P_1 and P_2 in the core*
p_c	=	*Capillary Pressure*			
P^S	=	*Pressure at saturation S*	x	=	*Position*
$P^S(P_{1,2},t_{1,2})$	=	*Pressures at two different times measured at sat. S in P_1 and P_2 for water and oil*	Δx	=	*Distance between P_1 and P_2*
			PV	=	*Pore Volume*
			q_w	=	*Water injection rate*
P_1	=	*Port 1*	P_2	=	*Port 2*

REFERENCES

[1] Johnson, E.F., Bossler, D.P., Naumann, V.O.: "Calculation of Relative Permeability from Displacement Experiments", *Petroleum Transactions* (1959), 216, p.370 – 372.

[2] Jones, S.C., Roszelle, W.O.: "Graphical Techniques for Determining Relative Permeability From Displacement Experiments", *Journal of Petroleum Technology* (1978), 30(5), p. 807 – 817.

[3] Kolltveit, K, Nordtvedt, J.E., Hovland, F., Kvanvik. B.A., Lie, B.: "Using Explicit and implicit Methods to Calculate Relative Permeabilities from In Situ Measurements", *Advances in Core Evaluation* (1990), p. 479 – 494.

[4] Helset, H.M., Skjæveland, S.M., Virnovsky, G.A.: "Application of composite membranes to determine relative permeabilities from displacement experiments", *Journ. of Petroleum Science and Eng."* (1998), **19**, p.81–91.

[5] Mejia, G.M., Mohanty, K.K., Watson, A.T.: "Use of in situ saturation data in estimation of two-phase flow functions in porous media", *Journal of Petroleum Science and Engineering"* (1995), **12**, p.233 – 245.

[6] Kokkedee, J.A., Boom, W., Frens, A.M., Maas, J.G.: "Improved Special Core Analysis: Scope for a reduced residual oil saturation", International Symposium of the Society of Core analysts, Montpellier, France, 1996.

[7] Honarpour, M.M., Cullick, A.S., Saad, N., Humphreys, N.V.: "Effect of Rock Heterogeneity on Relative Permeability: Implications for Scaleup", *Journal of Petroleum Technology* (1995), November, p.980 – 986.

[8] Lackner, A.S., Torsaeter, O.: "Phase pressure measurements: simultaneous and direct derivation of relative permeability and dynamic capillary pressure", International Symposium of the Society of Core analysts, Toronto, Canada, 2005.

[9] Bottero, S., Hassanizadeh, S.M., Kleingeld, P.J.: "From Local Measurements to an Upscaled Capillary Pressure-Saturation Curve", *Transp Porous Med* (2011), **88**, p. 271– 291.

[10] Schembre, J.M., Kovscek, A.R.: "A technique for measuring two-phase relative permeability in porous media via X-ray CT measurements", *Journal of Petroleum Science and Engineering"* (2003), **39**, p.159 – 174.

[11] Chardaire-Riviere, C., Chavent, G., Jaffre, J., Jun, L., Bourblax, B.J.: "Simultaneous Estimation of Relative Permeabilities and Capillary Pressure", *SPE Formation Evaluation* (1992), December, p.283 – 289.

[12] Goodfield, M., Goodyear, S.G., Townsley, P.H.: "New Coreflood Interpretation Method for Relative Permeabilities Based on Direct Processing of in-Situ Saturation Data", SPE Annual Technical Conference and Exhibition, New Orleans, Louisiana, USA, 2001.

[13] Brautaset, A., Ersland. G., Graue, A.: "In situ Phase Pressures and Fluid Saturation Dynamics Measured in Waterfloods at Various Wettability Conditions", *SPE Reservoir Evaluation and Eng.* (2010), June, p.465 – 472.

[14] Ekdale, A.A., Bromley, R.G.: "Trace Fossils and Ichnofabric in the Kjølby Gaard Marl, Uppermost Cretaceous, Denmark", *Bulletin of the Geological Society of Denmark* (1993), **31**, p.107 – 119.

[15] Fernø, M.A., Torsvik, M., Haugland, S., Graue, A.: "Dynamic Laboratory Wettability Alteration", *Energy and Fuels"* (2010), **24** (7), p. 3950 - 3958

[16] Amott, E.: "Observations Relating to the Wettability of Porous Rock", *Petroleum Transactions* (1959), **216**, p.156 – 162.

[17] Graue, A., Bognø, T., Moe, R.W., Baldwin, B.A., Spinler, E.A., Maloney, D., Tobola, D.P.: "Impacts of

Wettability on Capillary Pressure and Relative Permeability", International Symposium of the Society of Core Analysts, Golden, Colorado, USA, 1999.
[18] Craig, F.F.: "The Reservoir Engineering Aspects of Waterflooding", SPE, Austin, TX, USA, 1971.

Table 1: Fluid properties.

Fluid	Density [g/cm^3]	Viscosity [10^{-3} Pa·s]	Composition
Ekofisk D_20 brine	1.18	1.09	4.0% NaCl, 3.4% $CaCl_2$, 0.5% $MgCl_2$, 0.05NaN_3
n-Decane	0.73	0.92	-
Refined lamp oil	0.74	1.43	-
Decalin	0.90	0.85	-
Ekofisk Crude Oil	0.85	14.83	53% sat. HCs, 35% aromatics, 12% resins, 0.9% asphaltenes

Table 2: Core properties for Portland chalk core samples.

Core ID	Length [cm]	Diameter [cm]	Φ [%]	K [mD]	Aged [days]	Amott Index	Swi [%PV]	Sw,or [%PV]	Rf [%OOIP]
Core 1	8.0	5.08	47.4	4.87	0	1.00	31.6	68.2	48.4
Core 2	8.0	5.09	47.5	5.04	6	0.15	28.5	58.2	39.8
Core 3	7.5	5.10	46.7	4.89	6	0.08	24.4	64.3	52.6

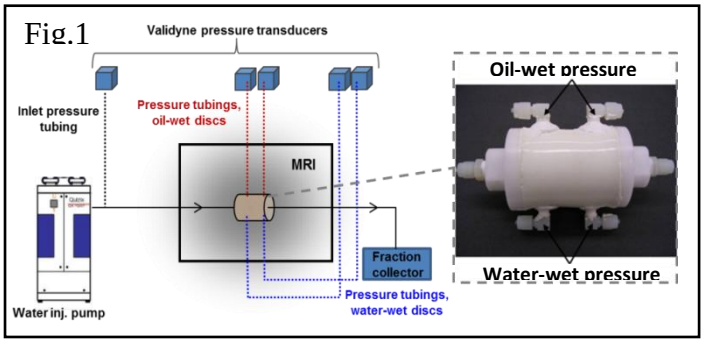

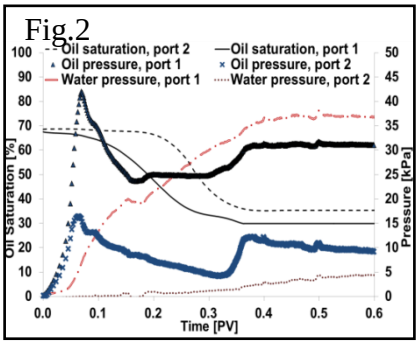

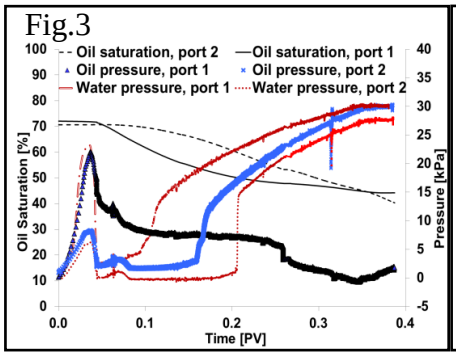

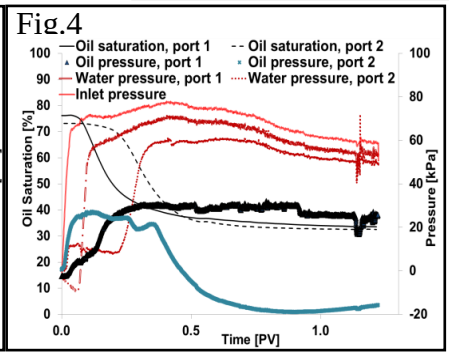

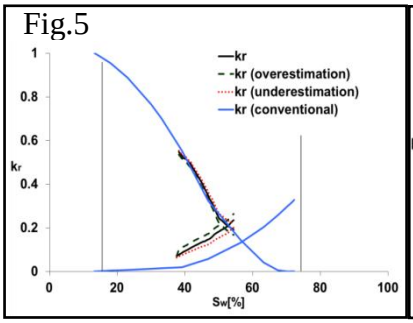

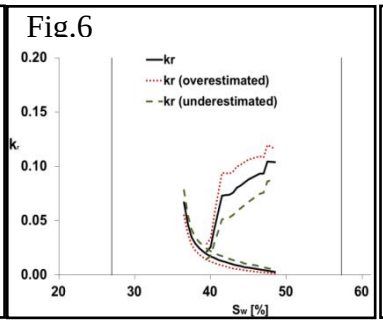

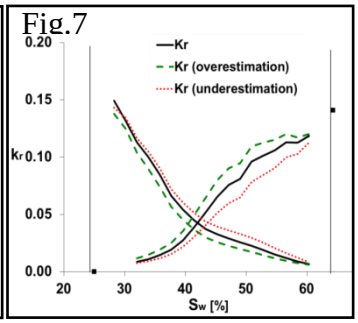

Figure 1: Schematic of the experimental setup. **Figure 2**: S_o, $P_o(t)$ and $P_w(t)$ at P_1 and P_2 locations during waterflooding of Core 1, Core 2 (**Figure 3**) and Core 3 (**Figure 4**). **Figure 5**: Relative permeabilities for Core 1, Core 2 (**Figure 6**) and Core 3 (**Figure 7**) calculated from *in-situ* data. The blue lines are relative permeabilities from conventional steady-state methods.